INVESTIGATION OF POINCARE SOLUTIONS OF NONLINEAR DUFFING AND PENDULUM UNDER SELECTED PERIODIC EXCITATIONS USING FRACTAL DISK CHARACTERISATION

ABSTRACT

Literature has shown that harmonically excited nonlinear Duffing and pendulum oscillators can respond chaotically under the influence of some of their drive parameters combination. However, there is scarcity of literature on the steady state responses of these oscillators when excited arbitrarily and periodically. Therefore, this research was designed to investigate the potential qualitative and quantitative variation in the steady Poincare solutions of nonlinear Duffing and pendulum oscillators under selected periodic excitations compared to their harmonically excited counterparts. The non-dimensional second Order Differential Equation (ODE) corresponding respectively to governing equation for harmonically/periodically excited nonlinear Duffing and pendulum were solved using the constant step fourth order Runge-Kutta algorithms. The corresponding steady state Poincare solutions obtained were characterized by both visual inspection and fractal dimension measure obtained using fractal disk counting method. Visual inspection of corresponding steady Poincare solutions show that they are qualitatively indistinguishable. However the corresponding estimated fractal dimension varied significantly.

The absolute variation in dimension was found to be between 4.92% and 1.37% for the Duffing oscillator and between 5.67% and 7.39% for the pendulum oscillator.

Keywords: *Excited Duffing Oscillator, Excited Pendulum Oscillator, Fourth-order Runge-Kutta, Fourier transformation, Periodic Excitation, Poincare section, and Fractal disk characterisation.*

1. INTRODUCTION

The behavior of a nonlinear system can be described by nonlinear systems equations which are a set of unknown differential equations. Nonlinearity is recognized as one of the principles of dynamics, and extensive research has been carried out in recent years. In particular, many studies have been based on the Duffing oscillator in different attempts to quantify and map the local and global dynamics of systems in which softening and hardening nonlinearities feature significantly (Lim, 2003).

Vibration isolators consisting of polymeric materials are used extensively in various forms of vibration control. Nonlinearities in these systems can arise from their geometrical effects, the mode of loading, and the material properties or combinations of all three (Lim, 2003). Polymeric material has been known to display softening nonlinearity in its stiffness and damping characteristics. They have also shown that the nonlinearity in the damping characteristic is seen to be more pronounced than that in the stiffness for these materials (Mallik et al, 1999).

Two fundamental nonlinear formulations based on two different strategies have been extended by Majed and Raynaud (2003) for the analysis of a nonlinear structure. The first formulation exploits the Eigen solutions of the associated linear system and the dynamic characteristics of each localised nonlinearity, while the second formulation was developed using the linearised Eigen solutions, which are calculated utilizing an iterative process (Lim, 2003). Their proposed formulation led to coherent results between theoretical and experimental results and was validated for two cases: the stiffness nonlinearity effects on transfer functions. The second one was on the stiffness and damping nonlinearity effects on transfer functions. Furthermore, the

strengthening of the stability of the solution around the resonance frequency was found to depend on several parameters, mainly the sine-sweep frequency, the weighting coefficient, and the convergence criteria.

In 1997, Luo and Han presented a method to determine the stability and bifurcations of a generalized Duffing oscillator. Finite terms of Fourier series have been used to approximate the analytic solution and the balance method to approximate the analytic solution of periodic motions in a periodically forced Duffing oscillator. In 1999, the analytical prediction of chaos in a nonlinear rod was investigated by Luo and Han. Luo (2004) developed the analytic conditions for chaotic motions in the resonant separatrix bands of a Mathieu Duffing oscillator. The numerical prediction was also completed through the energy increment spectrum method. Numerical solutions such as Euler's method and the Runge-Kutta method can also be used. The chaos and periodic motions are simulated by Poincare mapping. Luo (2012) developed a generalized harmonic balance method to approximate analytic solutions.

The Duffing attractor (an invariant set, as it has the same structure for different initial conditions in the basin of attraction that leads to chaotic trajectories) is a fine example of a so-called strange attractor due to its fractal structure. This is because the system is dissipative, so a flow evolved droplet of initial conditions will asymptomatically converge to a zero Lebesgue measure set (Morbidelli, 2002).

From the first scientific investigation by Galileo in 1602, the regular motion of the pendulum was used for timekeeping, and it was the world's most accurate timekeeping technology until 1930. Galileo discovered the crucial property that makes the pendulum a crucial timekeeper called isochronisms; the pendulum's period is approximately independent of the amplitude or width of the swing. Through the seventeenth, eighteenth, nineteenth, and early twentieth centuries, the pendulum played an essential role in developing classical mechanics. Santori invented a device that measured a patient's pulse by the pendulum's length. By the mid-20th century, the invention of digital computers led to an exponential increase in studying the mechanics of the pendulum. Today its interest cut across several fields, from science and engineering to education, military, civil, and industry, due to the broad range of applications (Han and Cao, 2016).

Since Galileo's first observations of the pendulum system, many researchers and authors have likewise studied the pendulum and applied its theory and principles to problems of repetitive or vibratory motion.

The angular displacement and its derivatives are the solutions to the governing equation of the pendulum. These solutions or the response of the pendulum could be periodic or otherwise. For a periodic response of the nonlinear pendulum, the solutions repeat at regular periods. Ozer and Akin (2005) also described the periodic response. In their work, they stated that the pendulum's response, when plotted, could be such that the displacement repeats in time at regular intervals. However, they stated that other forms of response are possible. Such other responses are described as aperiodic, non-periodic responses and could be chaotic, quasi-periodic, or almost periodic (Chau and Zheng, 2011). A quasi-periodic response will appear to have more than one type of behavior that it repeats. For example, it may have more than one maximum amplitude value of displacement that it repeats.

The Duffing equation has no exact solution (Elías-Zúñiga, 2006) but relies on approximate and numerical methods for its solution. The equation for the harmonically excited, nonlinear pendulum studied in this work is a nonlinear second-order differential equation. Such a nonlinear second-order differential equation, according to mathematical theory, is difficult or impossible to solve analytically (Chapra and Canale, 2006). Traditionally, researchers have used numerical means to obtain the solutions to this equation and then plotted it to visualize the pendulum response. Almost all sources from literature referred to in this work employed the Runge-Kutta Fourth Order numerical method to solve such differential equations. This is evidence of its popularity among researchers.

The second-order pendulum differential equation is first transformed into two first-order differential equations before numerical solution. After this, the resulting pair of coupled first-order ODEs are solved by appropriate numerical mathematical methods. In addition, according to the theory of numerical integration, the values of angular displacement and angular velocity obtained at the current iteration will depend on the values that were obtained during the previous iteration along with the time value for the current iteration. Furthermore, the time value at the current iteration depends on the time value for the previous iteration through the selected time discretization value or function (Tay et al, 2012).

The field of application of the Runge-Kutta methods in solving nonlinear higher-order equations is expanding. An example is a review of the development of the Runge-Kutta Discontinuous Galerkin (RKDG) methods for nonlinear convection-dominated problems carried out by Bernardo and Chi-Wang (2011). The review covered both the theoretical and algorithmic aspects of the methods. These methods combine a special class of Runge-Kutta time discretization that allows them to be nonlinearly stable regardless of the accuracy, with a finite element space discretization by discontinuous approximations that also incorporates the ideas of numerical fluxes and slope limiters coined during the remarkable development of the high-resolution finite difference and finite volume schemes.

The numerical solution of mathematical problems is highly iterative, with the number of iterations usually thousands. In order to overcome the tedium and fatigue this would cause if done manually by hand or with calculators, numerical solutions are usually carried out using a custom computer program (Chapra and Canale, 2006).

Chaos theory is a phenomenon that deals with the behavior of dynamical systems that are highly sensitive to slight differences in the initial conditions. Also, the term chaos has been described as sensitivity to minor differences in initial conditions. According to the French mathematician Henri Poincaré, in the description of what he termed chaos, "it may happen that small differences in the initial conditions produce very great ones in the final phenomena" (Chau and Zheng, 2011). Chaos is an essential feature of a nonlinear system. It is described as the response of a nonlinear pendulum to varying combinations of forcing amplitude and significant damping with force frequency held constant (Salau and Olabode, 2013). Many authors have studied the existence of period bifurcation and chaos in nonlinear externally driven oscillators. Many models that involve both additive excitation and parametric have been investigated with the restriction imposed by the numerical integration of the equation of motion (Diego and Oresto, 1983). Chaos control is the stabilization of unstable periodic orbits by means of small system perturbations to make them stable and predictable, which is more beneficial in chaos dynamics (Salau and Ajide, 2013).

The recent trend in the acceptance of chaotic diagrams as reliable visual tools in chaotic dynamics cannot be overemphasized (Salau and Ajide, 2013). Chaotic diagrams have been used by several researchers as a resourceful visual tool for qualitative explanations of some dynamic

systems that exhibits chaos. Chaotic vibrations of a harmonically excited nonlinear oscillator with Coulomb damping were investigated by numerical solution in a range of excitation frequencies (Narayanan and Jayaraman, 2003). A chaotic system could be studied by the use of different visual tools such as the state variables (time series), the phase portrait, the power spectrum, the Lyapunov exponents, the bifurcation diagram, and the Poincaré section. Using these tools, one can visually determine chaos's presence or onset, especially using bifurcation diagrams. In the work on introductory chaotic dynamics, Gregory and Jerry (1990) stated that for chaos to occur, there must be the existence of nonlinearity among at least three independent dynamical variables. In the work, they simulated the response of the nonlinear pendulum to a few chosen sets of input parameters. They also discussed the conditions for the onset and presence of chaotic response and the tools that are used to identify it.

The tools discussed include the bifurcation diagram, Lyapunov exponents, Spectral analysis, and Poincare section. The necessary conditions for chaotic motion are that (Ozer and Akin, 2005):- the system has at least three independent dynamical variables, and the equations of motion contain at least a nonlinear term.

In addition, a chaotic system is deterministic, in that the choice of initial conditions fully determines the state of the system at a future time. This dependence on initial conditions is otherwise expressed as sensitivity to minor differences in initial conditions (Chau and Zheng, 2011).

Fourier series is a way to represent a function as the sum of simple sine and cosine waves. Formally, it decomposes any periodic function or signal into the sum of a possibly finite set of simple oscillating functions, namely sines and cosines (or equivalently, complex exponentials). Early ideas of decomposing a periodic function into the sum of simple oscillating functions date back to the 3rd century BC, when ancient astronomers proposed an empiric model of planetary motions based on deferents and epicycles (Florian, 1893). The Fourier series is named in honor of Jean-Baptiste Joseph Fourier, who made important contributions to the study of trigonometric series after a preliminary investigation by Leonhard Euler, Jean le Rondd'Alembert, and Daniel Bernoulli. Fourier introduced the series for the purpose of solving the heat equation in a metal plate. Through Fourier's research, the fact was established that an arbitrary (continuous) function could be represented by a trigonometric series.

Fractals are mathematical objects that exhibit a self-similar pattern on every scale (Wikipedia, Fractal). Usually, they are manifolds that are nowhere differentiable. In order to describe fractals, the concept of dimension has to be extended to non-integer reals. Fractal geometry, in contrast, accommodates, regardless of complexity, all the shapes found in the real world without trying to force them to conform to any of the unnatural Euclidean shapes (Mandelbrot, 1983). Such real-world shapes include those of trees, coastlines, cloud formations, leaf venations, fruit shapes, speech signals, etc. In effect, while Euclidean geometry is limited in its application to analyze such complex and rough shapes, fractal geometry can handle all shapes regardless of complexity.

A fractal has been described as a rough or fragmented geometric shape that is capable of being divided into parts, with each part being approximately a reduced-size copy of the whole shape. This self-repeating property is popularly referred to as self-similarity. When a small piece of a fractal object is observed, it resembles a larger piece of the object or the object as a whole. Fractals are highly employed in computer modeling of irregular patterns and structures in nature (Salau and Ajide, 2012a) because of the fundamental property of fractals. This is because fractals themselves are geometric patterns that are repeated at ever smaller scales to produce irregular shapes and surfaces that cannot be represented by classical geometry.

Poincare Map is a tool for studying the asymptotic stability of periodic or almost periodic orbits. For example, suppose we have a planet that completes an orbit O (reference orbit)around the sun but slightly varies the orbit (neighboring orbits) each year (Sayan et al, 2014). A section is chosen to understand how the orbit varies. This section is called the Poincare section, and it must be transverse to the flow or the orbits. The Poincare section will be used to determine the chaos.

Therefore, the Poincare section simplifies the visualization of a complex shape without tampering with its underlying dynamics (Jacobo et al., 2009). Also, the Poincare section is similar to using a plane to cut through the trajectory of the fractal shape in phase space at regular intervals and make plot recordings of the points at which the fractal trajectory cuts the sectioning plan.

2. METHODOLOGY

2.1 Duffing Equation

The present study adopted the already reduced duffing equation (1). It is expressed in dimensionless form to reduce the number of adjustable parameters (Salau and Ajide, 2012).

$$\ddot{x} + \gamma\dot{x} - \frac{x}{2}(1 - x^2) = P_o \sin(\omega_D t) \qquad (1)$$

In equation (1), x, $\dot{x}$, $\ddot{x}$ represent displacement, velocity and acceleration of the oscillator about a datum point. Where 'γ' controls the amount of damping, P_o is the Amplitude strength of the harmonic excitation, ω_D is the excitation frequency, and t is the time (Guckenheimer & Holmes, 1983).

2.2 Periodic Excitation of Duffing Oscillator using Fourier transformation

The harmonic function $P_o \sin(\omega_D t)$ is converted to periodic, generalizing the terms, using fourier transformation. The Fourier series representing the function can be expressed as

$$f(t) = P_0 + \sum_{n=1}^{\infty}(P_n \cos \omega_n t + b_n \sin \omega_n t) \qquad (2)$$

Where $$P_0 = \frac{\omega}{\pi}\int_0^{\frac{2\pi}{\omega}} f(t)\, dt \qquad (3)$$

$$P_n = \frac{\omega}{\pi}\int_0^{\frac{2\pi}{\omega}} f(t)\cos \omega_n t \; dt \qquad (4)$$

$$Q_n = \frac{\omega}{\pi}\int_0^{\frac{2\pi}{\omega}} f(t)\sin \omega_n t \; dt \qquad (5)$$

In this research, two wave forms (periodic excitations) were considered.

2.2.1 Excitation

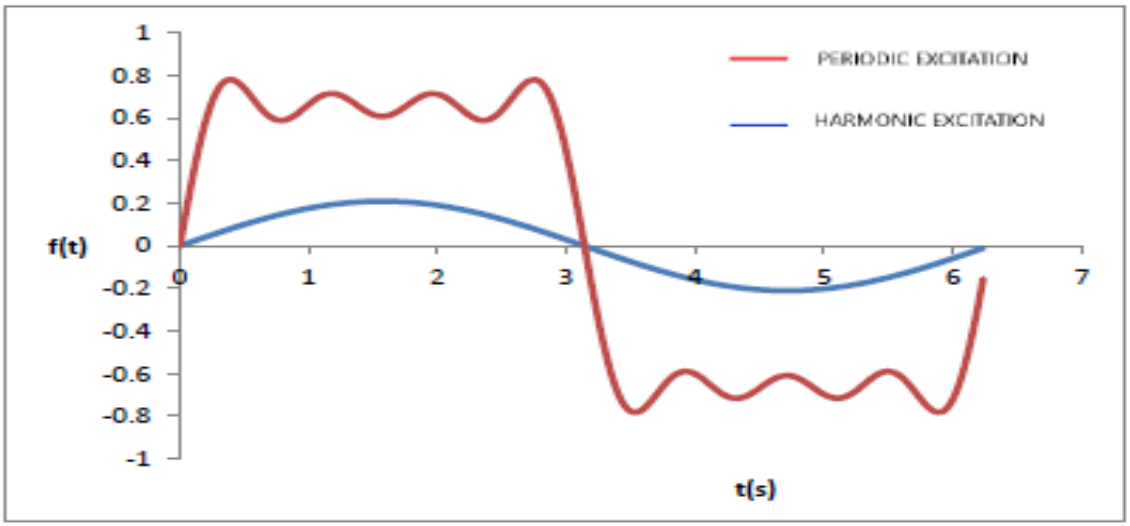

Figure 1: Periodic excitation 1 (square form) up to 7th term harmonics

Considering the periodic excitation 1, using fourier series, the forcing term required yielded;

$P_n = 0$

$Q_0 = 0$

$Q_n = 0$ (for all even n)

$Q_n = \frac{1}{n\pi}[1 - 2\cos(n\pi) + \cos(2n\pi)]$ (for all odd n) **(6)**

Rescaling the terms to have the same strength as the forcing amplitude,

$Q_n = \frac{Q_n}{Q_1} \times P_0$ (where P_0 is the Amplitude strength of the duffing oscillator)

$$f(t) = Q_1 \sin \omega_1 t + Q_3 \sin \omega_3 t + Q_5 \sin \omega_5 t + Q_7 \sin \omega_7 t \quad \textbf{(7)}$$

2.2.2 Excitation 2

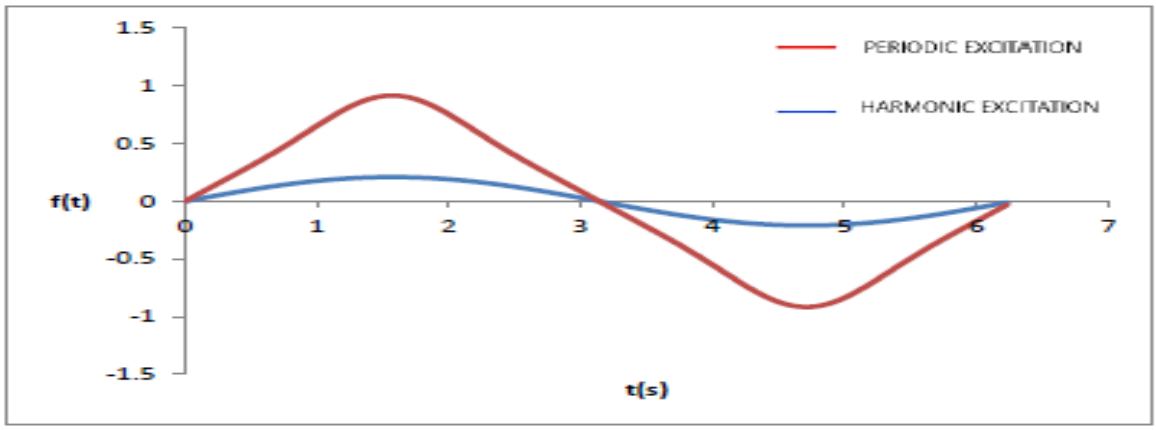

Figure 2: Periodic excitation (triangular form) up to 7th term harmonics

Considering the periodic excitation 2, using Fourier series, the forcing term required yielded;

$P_n = 0$

$Q_0 = 0$

$Q_n = 0$ (for all even n)

$Q_n = \frac{8}{(n\pi)^2} \sin\left(\frac{n\pi}{2}\right)$ (for all odd n) **(8)**

Rescaling the terms to have the same strength as the forcing amplitude,

$Q_n = \frac{Q_n}{Q_1} \times P_0$ (where P_0 is the Amplitude strength of the duffing oscillator).

The forcing term then is;

$$f(t) = Q_1 \sin \omega_1 t + Q_3 \sin \omega_3 t + Q_5 \sin \omega_5 t + Q_7 \sin \omega_7 t \quad \textbf{(9)}$$

2.3 Pendulum Equation

$$\frac{d^2\theta}{dt^2} + \frac{1}{q}\frac{d\theta}{dt} + \sin\theta = g\cos(\omega t) \quad \textbf{(10)}$$

It should be noted here that equation 10, is similar to the non-dimensional form of the forced nonlinear pendulum found in reviewed literature (Ozer and Akin, 2005), with a natural

oscillation frequency of unity applied. The number of adjustable parameters has been reduced to just three, that is the non-dimensional forcing amplitude (g), the non-dimensional damping factor (q) and the drive frequency (ω). Where $\theta, \frac{d\theta_1}{dt}, \frac{d^2\theta}{dt^2}$ are respectively, the angular displacement, undifferentiated), (angular velocity, first order differential) and (angular acceleration, second order differential).

2.4 Periodic Excitation of pendulum using Fourier transformation

The harmonic function g *cos* (ωt) is converted to periodic, generalizing the terms, using Fourier transformation. The Fourier series representing the function can be expressed as

$$f(t) = P_0 + \sum_{n=1}^{\infty}(P_n \cos \omega_n t + b_n \sin \omega_n t) \qquad \textbf{(11)}$$

Where $P_0 = \frac{\omega}{\pi} \int_0^{\frac{2\pi}{\omega}} f(t) \quad dt$ **(12)**

$$P_n = \frac{\omega}{\pi} \int_0^{\frac{2\pi}{\omega}} f(t) \cos \omega_n t \quad dt \qquad \textbf{(13)}$$

$$Q_n = \frac{\omega}{\pi} \int_0^{\frac{2\pi}{\omega}} f(t) \sin \omega_n t \quad dt \qquad \textbf{(14)}$$

In this research, two wave forms (periodic excitations) were considered.

2.4.1 Excitation 3

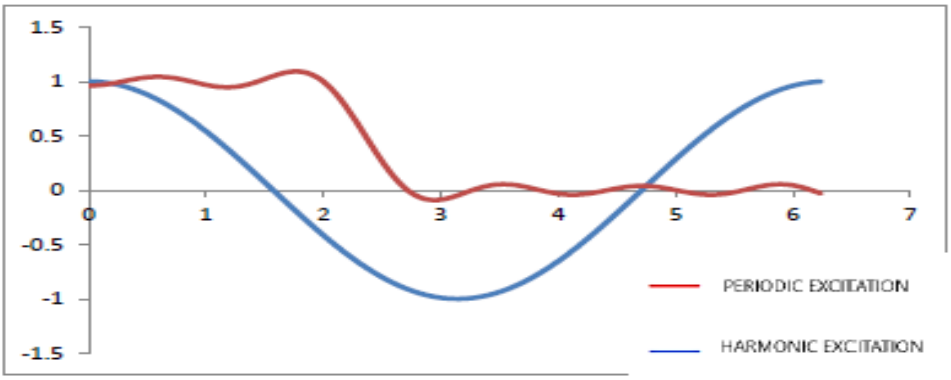

Figure 3: Periodic excitation 3 (square form) up to 7th term harmonics

Considering the periodic excitation 3, using Fourier series, the forcing term required yielded;

$Q_n = 0$

$P_0 = 1/2$

$P_n = 0$ (for all even n)

$P_n = \frac{2}{n\pi}[-1]^{\frac{n-1}{2}}$ (for all odd n) **(15)**

Rescaling the terms to have the same strength as the forcing amplitude,

$P_n = \frac{P_n}{P_1} \times g$

$$f(t) = \frac{1}{2} + P_1 \cos \omega_1 t + P_3 \cos \omega_3 t + P_5 \cos \omega_5 t + P_7 \cos \omega_7 t \quad \textbf{(16)}$$

2.4.2 Excitation 4

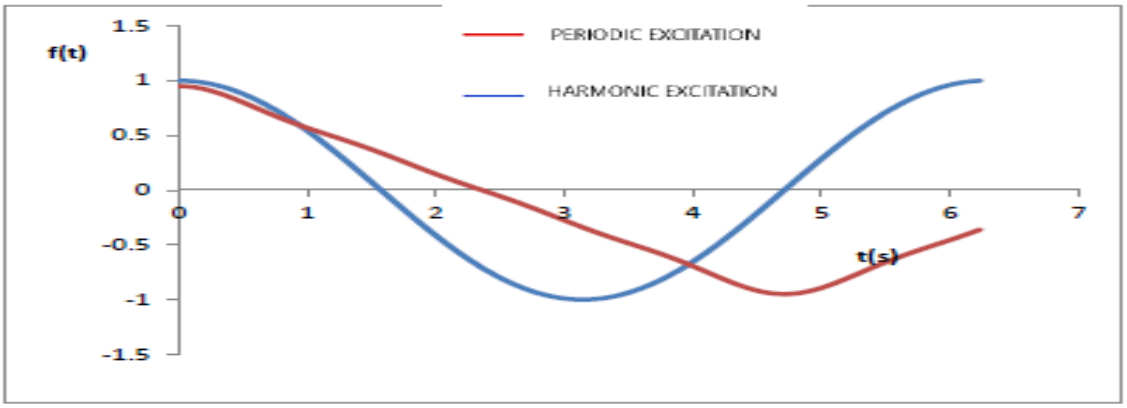

Figure 4: Periodic excitation (triangular form) up to 7th term harmonics

Considering the periodic excitation 4, using fourier series, the forcing term required yielded;

$Q_n = 0$

$P_0 = 0$

$P_n = 0$ (for all even n)

$P_n = 4[\frac{1-(-1)^n}{\pi^2 n^2}]$ (for all odd n) **(17)**

Rescaling the terms to have the same strength as the forcing amplitude,

$P_n = \frac{P_n}{P_1} \times g$ **(18)**

The forcing term then is;

$f(t) = P_1 \cos \omega_1 t + P_3 \cos \omega_3 t + P_5 \cos \omega_5 t + P_7 \cos \omega_7 t$ **(19)**

The present study utilised the popular constant operation time step fourth order Runge-Kutta schemes to simulate equation (1) in the first order rate of equations (2) and (3). The respective details of the scheme are provided in equations **(20)** to **(24)** substituting y for (θ_1,θ_2) , x for (t) and constant time step h.

2.5 Fourth-Order Runge-Kutta Scheme

$y_{i+1} = y_i + \frac{h}{6}[K_1 + 2(K_2 + K_3) + K_4]$ **(20)**

$K_1 = f(x_i, y_i)$ **(21)**

$K_2 = f\left(x_i + \frac{h}{2}, y_i + \frac{hK_1}{2}\right)$ **(22)**

$K_3 = f\left(x_i + \frac{h}{2}, y_i + \frac{hK_2}{2}\right)$ **(23)**

$K_4 = f(x_i + h, y_i + hK_3)$ **(24)**

2.6 Study parameters

2.6.1 Duffing Oscillator

From literature research, this study focuses on the parameters defined by; the non-dimensional forcing amplitude (P_o = 0.168), damping constant (γ = 0.21). Simulation of these parameters was carried out over the drive frequency ω_Dt = 1. The simulation time step is fixed at h= $\frac{T_P}{500}$for

$T_P = \frac{2\pi}{\omega_D}$ and the initial conditions for studied cases is (0, 0). The simulation was executed for 2000-excitation periods (i.e. $10T_P - 2010T_P$).

2.6.2 Pendulum Oscillator

From literature research, this study focuses on the parameters defined by; damping qualities

(q) =4.0, drive amplitude (g) $= 1.5$ and frequency $(\omega_D) = 2/3$. The simulation time step is fixed at h= $\frac{T_P}{500}$for $T_P = \frac{2\pi}{\omega_D}$ and the initial conditions for studied cases is (0, 0). The simulation was executed for 2000-excitation periods (i.e. $10T_P - 2010T_P$).

3. RESULTS AND DISCUSSION

3.1 Duffing Oscillator

The Poincare patterns in figure 3 compare excellently well with those reported by Salau and Ajide (2012), amplitude (P_o = 0.168), damping constant (γ = 0.21) fixed drive frequency of 2/3. Figures 4 and 5 show the Poincare solutions (scatter plots), with attractor layout of periodically excited duffing oscillator using a fractal disk scale of 2. The scatter plots distribution per unit space area varies non-uniformly from one location to another. This shows that nonlinear duffing oscillators under periodic excitations are chaotic.

Tables 1-3 show the variation of optimum counted disks with increasing observation scale number for the referenced harmonic excitation and the periodic excitation simulation periods.

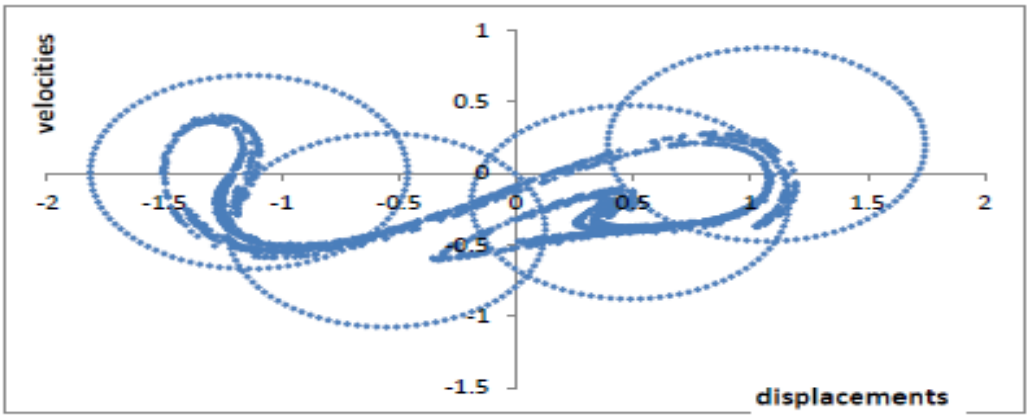

Figure 5: Poincare section of harmonically excited duffing oscillator showing the attractor layout for scale 2 disk.

Table 1: The generated report (10 trials) of disk laying of the Poincare (harmonic excitation)

Scale	Optimum disk count	Trial 1	Trial 2	Trial 3	Trial 4	Trial 5	Trial 6	Trial 7	Trial 8	Trial 9	Trial 10
1	2	2	3	2	2	2	2	2	2	2	2
2	4	6	5	4	5	5	4	4	5	4	5
3	8	9	8	8	9	9	8	8	8	9	8
4	12	12	12	14	12	12	13	15	12	12	12
5	16	17	20	19	18	16	19	17	18	17	18
6	21	23	24	23	21	22	22	23	21	22	23
7	23	28	28	27	23	27	28	27	28	29	26
8	29	32	31	32	33	33	30	33	34	34	29
9	36	36	40	40	39	39	37	40	38	38	38
10	40	41	45	40	44	46	41	41	45	43	44

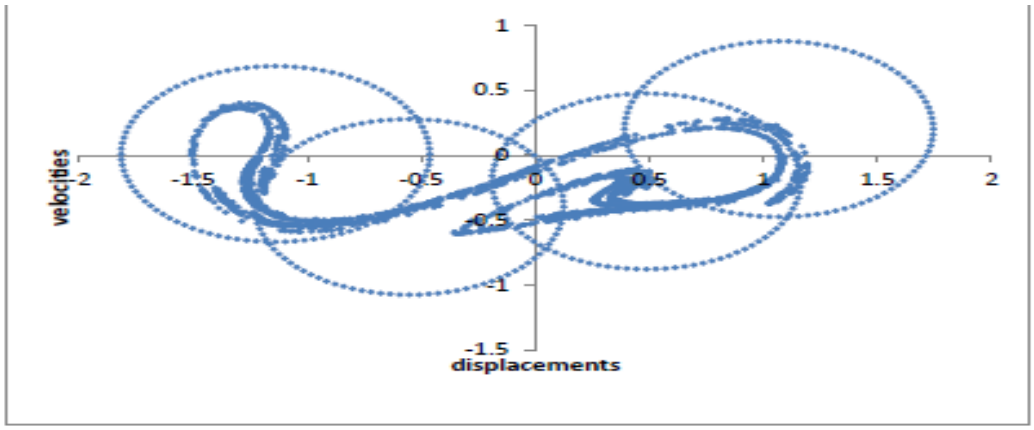

Figure 6: Poincare section of periodically excited duffing (excitation 1) showing the attractor layout for scale 2 disk

Table 2: The generated report (10 trials) of disklaying of the Poincare (periodic excitation 1)

Scale	Optimum disk count	Trial 1	Trial 2	Trial 3	Trial 4	Trial 5	Trial 6	Trial 7	Trial 8	Trial 9	Trial 10
1	2	2	2	2	2	2	2	2	2	2	2
2	4	5	5	6	5	4	4	6	6	6	5
3	8	9	10	8	9	9	9	9	9	9	9
4	12	13	13	12	12	14	14	15	14	14	14
5	17	18	20	18	19	17	21	20	18	18	18
6	21	23	24	21	24	26	23	22	25	24	25
7	28	31	29	32	29	31	30	33	32	28	32
8	33	39	36	33	35	38	35	34	34	36	35
9	41	43	44	41	43	47	42	45	43	43	44
10	44	45	49	49	46	44	47	50	51	46	51

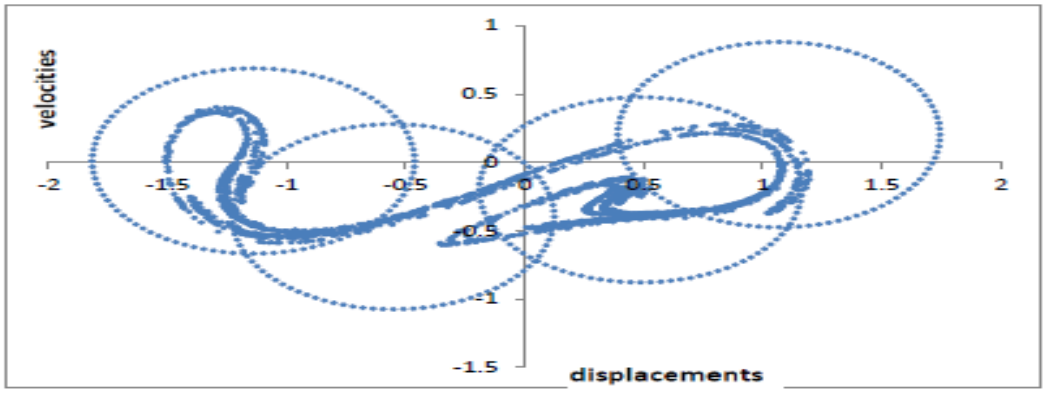

Figure 7: Poincare section of periodically excited duffing (excitation 2) showing the attractor layout for scale 2 disk.

Table 3: The generated report (10 trials) of disk laying of the Poincare (periodic excitation 2)

Scale	Optimum disk count	Trial 1	Trial 2	Trial 3	Trial 4	Trial 5	Trial 6	Trial 7	Trial 8	Trial 9	Trial 10
1	2	3	3	2	3	3	3	3	3	3	2
2	4	5	5	5	6	5	5	5	5	4	4
3	8	10	9	10	9	8	9	9	8	9	9
4	13	15	14	14	14	14	14	13	13	14	13
5	16	17	17	16	18	16	18	16	17	18	16
6	20	21	21	20	23	22	22	22	21	21	21
7	25	27	25	26	26	26	27	25	26	26	26
8	29	31	31	30	30	31	30	29	29	31	31
9	34	35	35	38	36	37	36	37	34	39	34
10	37	44	37	43	38	40	40	40	42	42	44

Table 4: Disk count and Logarithm of disk count

	Disks Counted			Natural Logarithms			
Observation Scales	Harmonic Excitation	Periodic Excitation I	Periodic Excitation II	Observation Scales	Harmonic Excitation	Periodic Excitation I	Periodic Excitation II
1	2	2	2	0.00	0.69	0.69	0.69
2	4	4	4	0.69	1.39	1.39	1.39
3	8	8	8	1.10	2.08	2.08	2.08
4	12	12	13	1.39	2.48	2.48	2.56
5	16	17	16	1.61	2.77	2.83	2.77
6	21	21	20	1.79	3.04	3.04	3.00
7	23	28	25	1.95	3.14	3.33	3.22
8	29	33	29	2.08	3.37	3.50	3.37
9	36	41	34	2.20	3.58	3.71	3.53
10	40	44	37	2.30	3.69	3.78	3.61

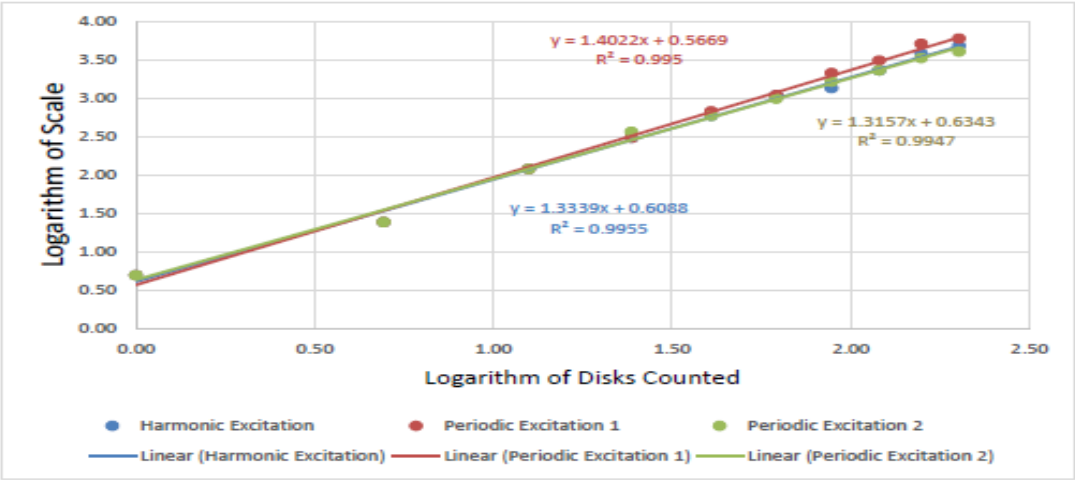

Figure 8: Log=Log plots of disks required for the overlay

Table 4 shows a sample of optimum variation of disks counted for ten (10) different observations scale for the three (3) investigated cases. The slope of line of best fit in figure 8 is an expression of the fractal quantification of space filling ability of the Poincare given in figures 5, 6 and 7.

Figure 7 (triangular wave form excitation) with estimated fractal disk dimension values of 1.315, coefficient of fitness (R^2=0.994) is quite similar quantitatively to that of the harmonic excitation (figure 5) which has an estimated dimension value of 1.333 and a coefficient of fitness (R^2=0.995). It can be argued that the Poincare produced by the square wave form periodic excitation fill space more than both the Poincare produced by the harmonic and the triangular wave form. Its estimated fractal disk dimension value is 1.2553 with coefficient of fitness (R^2=0.997).

3.2 Pendulum Oscillator

The Poincare patterns in figure 9 compare excellently well with those reported by Gregory and Jerry (1990) for damp quality 4, fixed excitation amplitude of 1.5 and fixed drive frequency of 2/3. Figures 10 and 11 show the Poincare solutions (scatter plots), with attractor layout of periodically excited pendulum using a fractal disk scale of 2. The scatter plots distribution per unit space area varies non-uniformly from one location to another. This shows that nonlinear pendulums under periodic excitations are chaotic.

Tables 5-7 show the variation of optimum counted disks with increasing observation scale number for the referenced harmonic excitation and the periodic excitation simulation periods.

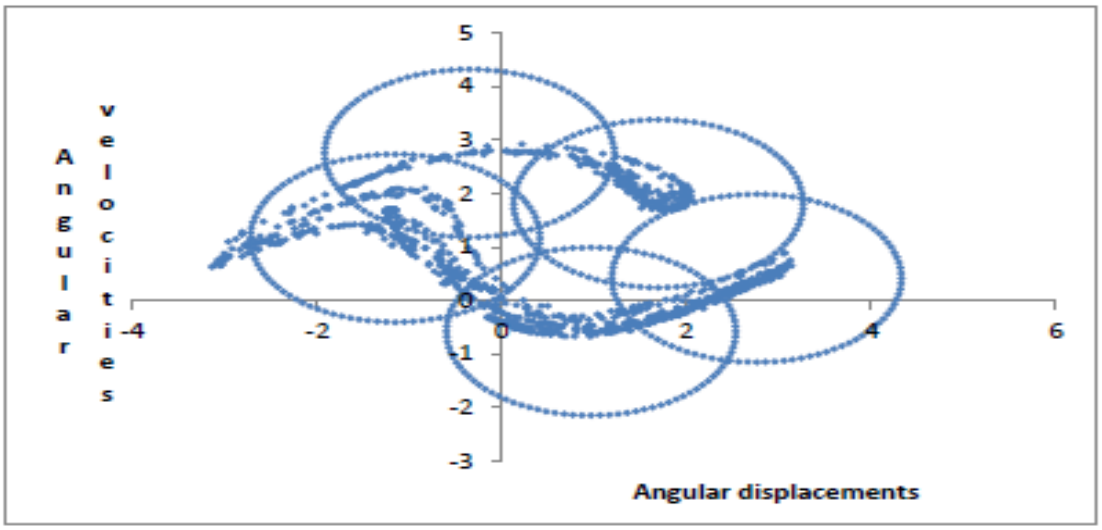

Figure 9: Poincare section of harmonically excited pendulum showing the attractor layout for scale 2 disk

Table 5: The generated report (10 trials) of disk laying of the Poincare (harmonic excitation)

Scale	Optimum disk count	Trial 1	Trial 2	Trial 3	Trial 4	Trial 5	Trial 6	Trial 7	Trial 8	Trial 9	Trial 10
1	2	2	2	3	2	3	3	2	2	2	3
2	5	6	6	6	5	6	7	6	6	6	6
3	9	9	9	10	10	9	9	9	9	9	9
4	12	14	12	13	12	12	13	13	12	12	12
5	15	16	17	16	16	17	16	16	15	15	17
6	18	20	22	20	18	20	20	21	19	21	20
7	23	24	24	23	26	23	25	24	23	26	23
8	28	29	28	30	30	30	29	28	30	31	28
9	33	37	34	36	33	35	35	37	34	36	36
10	39	39	41	40	40	43	40	40	40	42	40

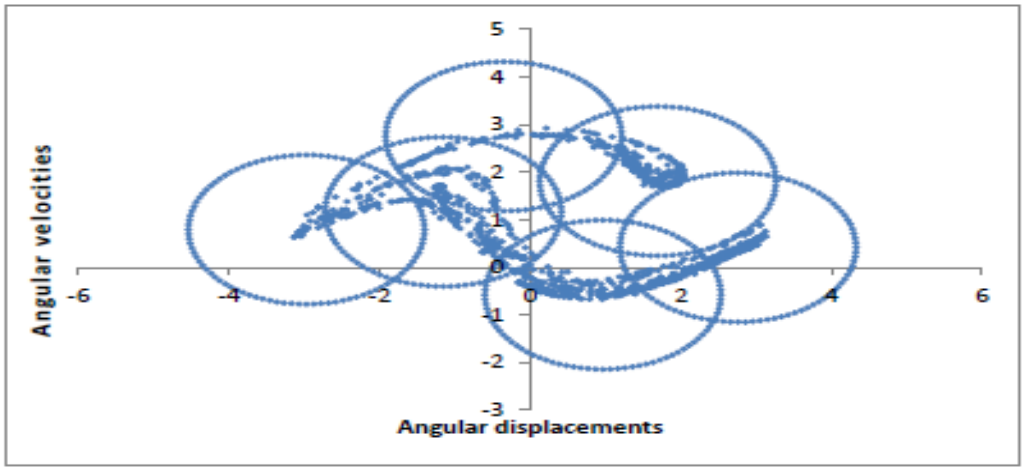

Figure 10: Poincare section of periodically excited pendulum (excitation 1) showing the attractor layout for scale 2 disk

Table 6: The generated report (10 trials) of disk laying of the Poincare (periodic excitation 1)

Scale	Optimum disk count	Trial 1	Trial 2	Trial 3	Trial 4	Trial 5	Trial 6	Trial 7	Trial 8	Trial 9	Trial 10
1	2	3	2	2	2	2	3	3	2	3	2
2	6	6	7	6	6	6	6	6	6	7	6
3	8	10	10	10	9	9	9	8	9	10	9
4	12	14	13	14	13	14	13	15	14	12	13
5	17	17	19	19	19	19	18	18	17	19	18
6	20	20	25	24	26	24	23	26	26	23	23
7	28	30	32	30	33	30	29	30	31	30	28
8	35	36	35	38	39	36	36	38	37	36	40
9	41	44	45	43	47	46	44	41	49	41	47
10	49	52	52	55	51	50	50	51	49	51	54

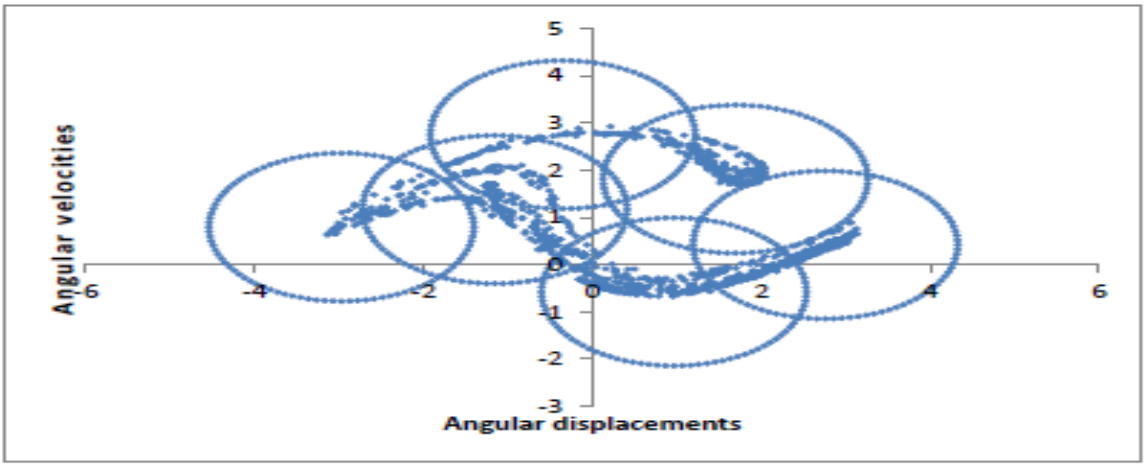

Figure 11: Poincare section of periodically excited pendulum (excitation 2) showing the attractor layout for scale 2 disk.

Table 7: The generated report (10 trials) of disk laying of the Poincare (periodic excitation 2)

Scale	Optimum disk count	Trial 1	Trial 2	Trial 3	Trial 4	Trial 5	Trial 6	Trial 7	Trial 8	Trial 9	Trial 10
1	2	2	2	3	2	2	2	3	3	2	2
2	6	6	7	6	6	7	7	6	6	7	7
3	8	9	11	8	8	9	8	9	9	9	10
4	12	14	12	13	12	12	14	12	12	14	14
5	17	18	18	19	18	18	18	17	20	18	19
6	21	22	21	22	25	23	23	21	23	23	24
7	26	29	27	29	29	26	28	27	28	27	30
8	32	34	37	35	32	32	38	35	36	37	36
9	39	42	39	41	41	42	41	39	43	46	45
10	48	52	55	50	49	51	53	50	51	49	48

Table 8: Disk count and Logarithm of disk count

	DISKS COUNTED			NATURAL LOGARITHMS			
Observation Scales	Harmonic Excitation	Periodic Excitation I	Periodic Excitation Ii	Observation Scales	Harmonic Excitation	Periodic Excitation I	Periodic Excitation II
1	2	2	2	0.00	0.69	0.69	0.69
2	5	6	6	0.69	1.61	1.79	1.79
3	9	8	8	1.10	2.20	2.08	2.08
4	12	12	12	1.39	2.48	2.48	2.48
5	15	17	17	1.61	2.71	2.83	2.83
6	18	20	21	1.79	2.89	3.00	3.04
7	23	28	26	1.95	3.14	3.33	3.26
8	28	35	32	2.08	3.33	3.56	3.47
9	33	41	39	2.20	3.50	3.71	3.66
10	39	49	48	2.30	3.66	3.89	3.87

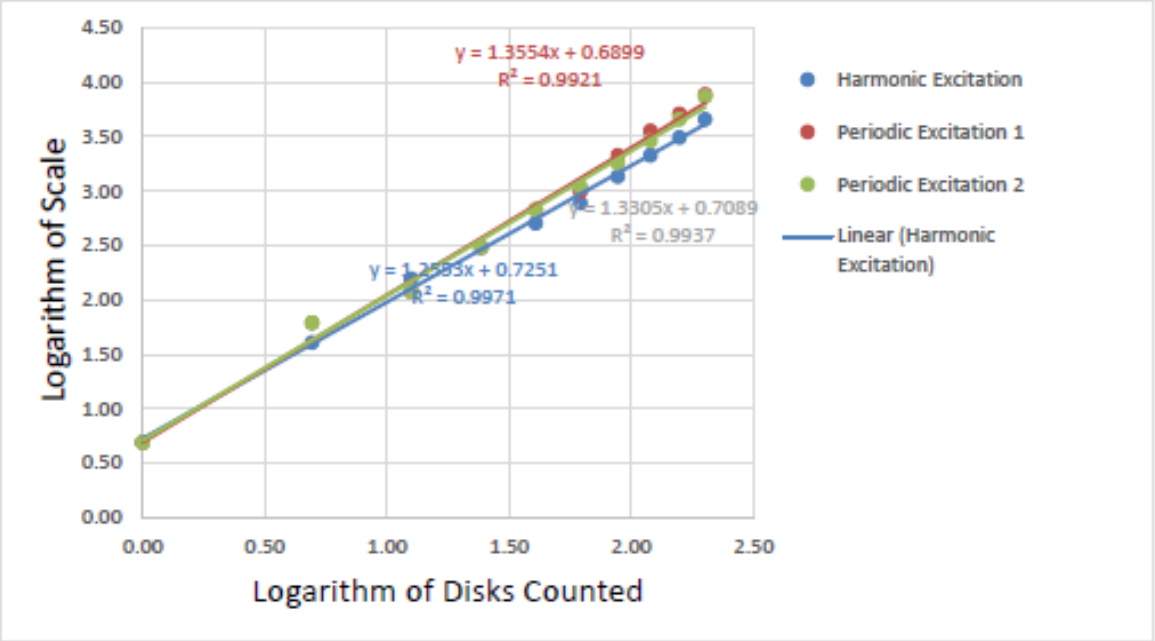

Figure 12: Log plots of disks required for the overlay

Table 8 shows a sample of optimum variation of disks counted for ten (10) different observations scale for the three (3) investigated cases. The slope of line of best fit in figure 12 is an expression of the fractal quantification of space filling ability of the Poincare given in figures 9, 10 and 11.

Therefore, it can be argued that figures 10 and 11 with estimated fractal disk dimension values of 1.3554, coefficient of fitness (R^2=0.9921) and 1.3305, coefficient of fitness (R^2=0.993) respectively, fill space more than figure 9 with estimated fractal disk dimension value of 1.2553 with coefficient of fitness (R^2=0.997).

4. CONCLUSIONS

Qualitatively, the effect of periodic excitation on the duffing system is the same as that of the harmonic excitation on it. However, the number of disks required to cover the Poincare varied from harmonic to periodic excitations. This implies that the effects are quite different quantitatively. Under the harmonic excitation, the Poincare has a dimension of 1.333 and under the selected periodic excitations, the fractal dimensions are 1.402 and 1.315. This implies that the Poincare of the periodically excited duffing (square waveform) occupied more space on the 2D-

euclidean space than that of the harmonically excited duffing. The absolute variation in dimension is between 4.92% and 1.37%.

Qualitatively, the effect of periodic excitation on the pendulum system is the same as that of the harmonic excitation on it. However, the number of disks required to cover the Poincare varied from harmonic to periodic excitations. This implies that the effects are quite different quantitatively. Under the harmonic excitation, the Poincare has a dimension of 1.2553 and under the selected periodic excitations, the fractal dimensions are 1.3554 and 1.3305. This implies that the Poincare of the periodically excited pendulum occupied more space on the 2D-euclidean space than that of the harmonically excited pendulum. The variation in dimension is between 5.67% and 7.39%. Therefore, the effect of periodic excitations on dynamic systems should also be of interest as there is a relatively large difference.

REFERENCES

[1] Bernardo, C. and Chi-Wang, S., (2011). Runge-Kutta Discontinuous Galerkin Methods for Convection Dominated Problems. Journal of Scientific Computing, 16(3): 173-261.

[2] Chapra, S.C. and Canale, R.P. (2006), Numerical Methods for Engineers, fifth edition, McGraw-Hill (International Edition), New York, ISBN 007-124429-8, pp. 142, 700, 727, 733, 875.

[3] Chau, K.T and Zheng, W., (2011), Chaos in Electric Drive Systems: Analysis, Control and Application, John Wiley & Sons. Ltd., ISBN 978-0-470-82633-1, pp. 4.

[4] Diego L. Gonzalez and OrestoPiro, (1983), Chaos in a Nonlinear Driven Oscillator with Exact Soluton. Physical review letter volume 50 number 12.

[5] Elías-Zúñiga, A., 2006. A General Solution of the Duffing Equation. Nonlinear Dyn. 45, 227–235. doi:10.1007/s11071-006-1858-z.

[6] Florian Cajori, A History of Mathematics (1893) p. 283.

[7] Han, Ning, and Qingjie Cao. 2016. “Rotating Pendulum with Smooth and Discontinuous Dynamics.” International Journal of Mechanical Sciences.

[8] Jacobo, A., Ricardo, L.V. and Miguel, A.F.S., (2009). Fractal structures in nonlinear dynamics. American Physical Society’s New Journal. 81(1): 333-386.

[9] Lim,FannonChwee Ning (2003) A preliminary investigation into the effects of nonlinear response modification within coupled oscillators. PhD thesis.

[10] Luo ACJ, Han RPS. A quantitative stability and bifurcation analysis of a generalized Duffing oscillator with strong nonlinearity, Journal of Sound and Vibration 1997; 334B:447-459.

[11] Luo ACJ, Huang JZ. Approximate solutions of periodic motions in nonlinear systems via a generalized harmonic balance. Journal of Vibration and Control 2012; 18: 1661-1871.

[12] Luo ACJ. Chaotic notion in the resonant separatrix bands of a Mathiue-Duffing oscillatorwith twin-well potential, Journal of Sound and Vibration 2004; 273:653-666.

[13] Majed R. and Raynaud J. L. (2003), Journal of Sound and Vibration Analysis of a non-linear structure by considering two non-linear formulations. doi: 10.1016/S0022 460X(02)00930-6, 260(5), 847-866.

[14] Mallik A K, Kher V, Puri M. and Hatwal H. (1999), Journal of Sound and Vibration 219(2), 239-253. On the modelling of non-linear elastomeric vibration isolators. doi: 10.1006/jsvi. 1998.1883.

[15] Morbidelli .A, Modern Celestial Mechanics, CRC Press, 2002.

[16] Özer, A.B. and Akin, E., (2005). Tools for detecting chaos, SAÜ Fen BilimleriEnstitüsüDergisi. Cilt, 1. Sayõ 2005, pp 60-66, FiratÜniv. Müh. Fak. BilgisayarMüh. Böl. ELAZIĞ.

[17] Salau T. A.O. and Ajide O.O (2013). A Novel Graphic Presentation and Fractal characterization of Poincare Solution of Harmonically Excited Pendulum. International Journal of Advances in Engineering & Technology, July 2013.

[18] Salau T.A.O & Olabode A.A(2013) Fractal characterization and Iso-mapping of Parameter Plane of Harmonically Excited Pendulum. International Journal of Scientific & Engineering Research, Volume 4, Issue 7, July-2013 790 ISSN 2229-5518.

[19] Salau T.A.O. and Ajide O.O. (2012(a)), Comparative Analysis of Time Steps Distribution in Runge-Kutta Algorithms, International Journal of Scientific & Engineering Research Volume 3, Issue 1, January-2012 1 ISSN 2229-5518.

[20] Tay, K.G., Kek, S.L. and Abdul-Kahar, R., (2012). A Spreadsheet Solution of a System of Ordinary Differential Equations Using Fourth-Order Runge-Kutta Method. Spreadsheets in Education (eJSiE), vol 5(2).